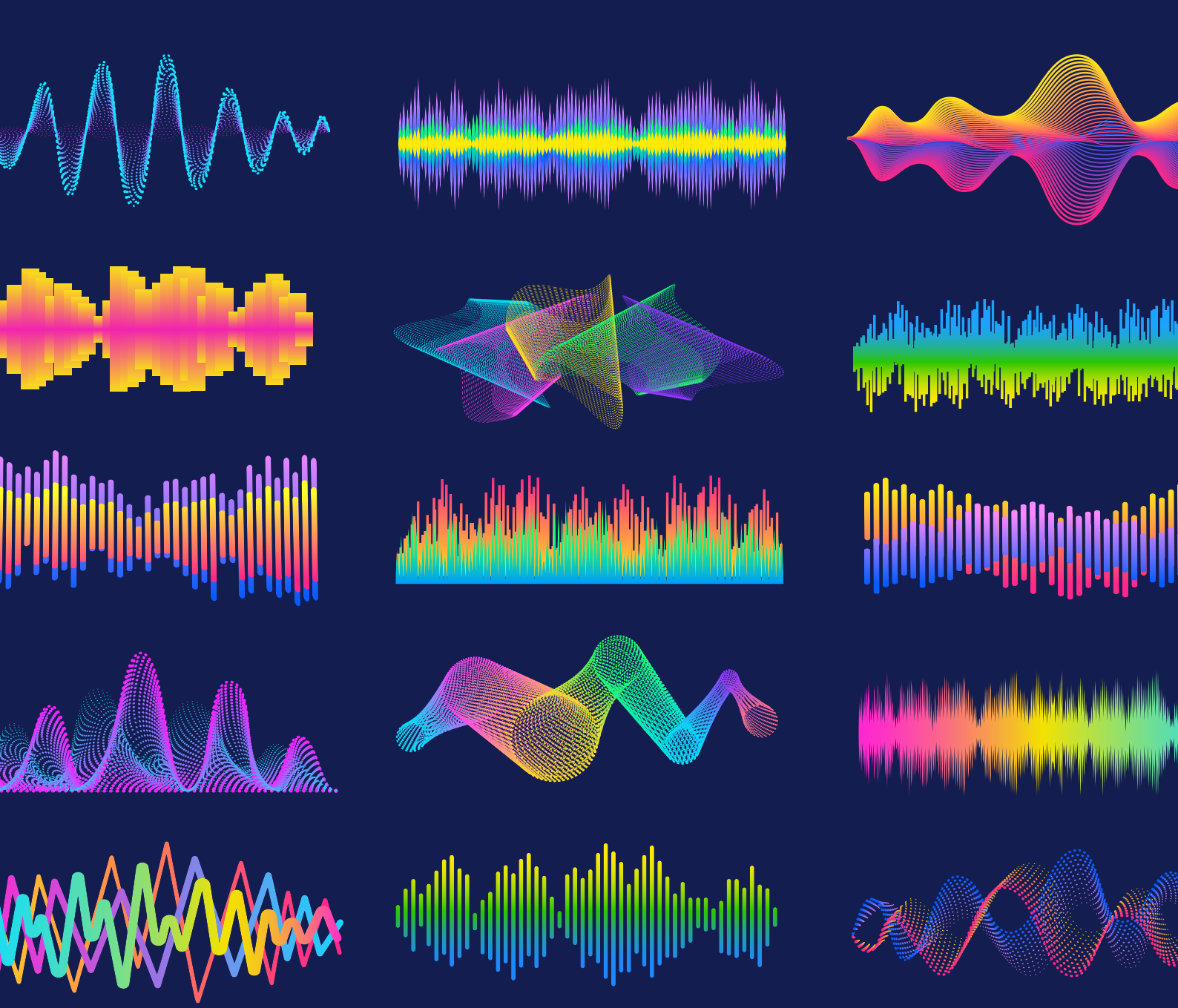


Portable Ultrasound System for Blood Velocity Estimation

Jeppe Hinrichs

Master Thesis



Contents

Contents	III
List of Figures	IV
List of Tables	V
Abbreviations	VI
Glossary	VII
Nomenclature	VIII
1 Introduction	1
1.1 Project scope	2
2 Theory	5
2.1 Ultrasound	5
2.1.1 Scattering	6
2.1.2 Attenuation	7
2.1.3 Transducer	8
2.1.4 Doppler effect	8
2.2 Flow physics	10
2.2.1 Blood flow	12
2.3 Devices	12
2.3.1 Continuous-wave flowmeter	13
2.3.2 Pulsed-wave flowmeter	15
3 Synthesis	17
3.1 Graphs and charts	17
3.2 Tables and figures	20
3.3 Equations	22
3.4 Listings (code)	23
Bibliography	25
A Bill of Materials	28
B Instruments	31

List of Figures

2.1	Particle displacement for a propagating ultrasound wave	5
2.2	Single element ultrasound transducer construction	8
2.3	Transducer types for acquiring B-mode images	9
2.4	Doppler effect diagram	10
2.5	Circulatory system of the human body	11
2.6	Diagram of ultrasound wave transmitted and reaching blood vessel with incident angle θ	12
2.7	Block diagram of continuous-wave flowmeter	13
2.8	Doppler signals in time and frequency domain showing demodulation effects	14
2.9	Block diagram of pulsed-wave flowmeter	15
2.10	Sampling for a gate pulsed wave system with a single range	16
3.1	Simplified overview of the system	17
3.2	Stacked column chart	17
3.3	Stacked bar chart	18
3.4	Grouped column chart	18
3.5	Line graph	18
3.6	Line graph with magnifying glass	19
3.7	Area graph	19
3.8	Scatter plot	19
3.9	Boxplot	20
3.10	The nodes short, V, R and L are presented here, but there a lot more	20
3.11	Just a normal figure	21
3.12	A figure with two subfigures	22
3.13	A figure with four subfigures	22

List of Tables

3	Nomenclature	VIII
1.1	Comparison of medical imaging modalities	1
1.2	Project specification table	2
2.1	Approximate density, sound speed, and acoustic impedance of human tissue types	6
2.2	Approximate attenuation values for human tissue	7
2.3	Measured frequency shifts with a Doppler 3 MHz transducer at various velocities at a 45° incident angle	15
3.1	This is a <code>booktabs</code> table	20
3.2	Wrongly formatted table	21
3.3	Correctly formatted table	21
A.1	BOM	28
B.1	List of instruments used for solder work	31
B.2	List of instruments used for testing	31

Abbreviations

Notation	Description
<i>ADC</i>	analogue-to-digital converter
<i>BP</i>	band-pass
<i>CT</i>	computed tomography
<i>CW</i>	continuous-wave
<i>DTU</i>	Danmarks Tekniske Universitet (Technical University of Denmark)
<i>KAIST</i>	Korea Advanced Institute of Science and Technology
<i>low-res</i>	low resolution
<i>MRI</i>	magnetic resonance imaging
<i>PSD</i>	power spectral density
<i>PW</i>	pulsed-wave
<i>US</i>	ultrasound

Glossary

Notation	Description
adiabatic	Any process that happens without heat gain or loss is considered adiabatic
Doppler effect	A change in frequency of a wave in relation to an observer who is moving relative to the wave source
transcutaneous	Applied across the depth of the skin without invasive penetration

Nomenclature

Table 3: Nomenclature

Name	Unit	Description
Input filter		
V_{ref}	V	Reference voltage
C_{hp}	F	High pass filter capacitor
R_{hp}	Ω	High pass filter resistor
f_{hp}	Hz	High pass cut-off frequency
C_{lp}	F	Low pass filter capacitor
R_{lp}	Ω	Low pass filter resistor
f_{lp}	Hz	Low pass cut-off frequency
A_v	1	Amplification factor
Modulator		
R_1	Ω	AIM voltage divider resistor
R_2	Ω	AIM voltage divider resistor
R_{in}	Ω	AIM input resistor
R_{fb}	Ω	AIM feedback resistor
C_1	F	AIM capacitor
V_{in}	V	Input signal voltage
V_{span}	V	Voltage range of input signal
V_{pwm}	V	PWM signal
V_H	V	V_{pwm} high level voltage
V_L	V	V_{pwm} low level voltage
V_{out}	V	V_{pwm} voltage range ($V_H - V_L$)
V_{hys}	V	Hysteresis voltage
V_{hw}	V	Hysteresis width
V_{th_H}	V	Hysteresis threshold upper voltage
V_{th_L}	V	Hysteresis threshold lower voltage
V_c	V	PWM carrier voltage
V_{c_H}	V	PWM carrier upper voltage
V_{c_L}	V	PWM carrier lower voltage
f_{sw}	Hz	PWM signal frequency
D	1	PWM signal duty cycle

Continued on next page

Table 3: Nomenclature (Continued)

Name	Unit	Description
t_H	s	PWM carrier charge time
t_L	s	PWM carrier discharge time
τ	1	PWM carrier charge constant
R_{th}	Ω	PWM carrier thevenin resistance
f_{idle}	Hz	PWM signal idle switching frequency
k_2	1	R_{fb} , R_{in} voltage divider
Gate driver		
D_{dt}	1	Dead-time circuit diode
R_{dt}	Ω	Dead-time circuit resistor
C_{dt}	F	Dead-time circuit capacitor
V_C	V	Dead-time circuit supply voltage
V_s	V	IC supply voltage
t_c	s	Charging circuit time
Power stage		
V_{DD}	V	Power supply voltage
Q_1, Q_2, Q_3, Q_4	1	Power stage switches
V_g	V	Gate driver signal
V_o	V	Output voltage
I_o	A	Output current
R_{BTL}	Ω	Speaker equivalent load resistance
Output filter		
R_f	Ω	Output filter single-ended load
C_{BTL}	F	Output filter differential capacitance
C_f	F	Output filter single-ended capacitance
L_f	H	Output filter inductance
ΔI_L	A	Output filter ripple current
Q	1	Output filter quality factor
f_c	Hz	Output filter cut-off frequency
ω_n	rads^{-1}	Output filter natural frequency
ζ	1	Output filter damping ratio

Continued on next page

Table 3: Nomenclature (Continued)

Name	Unit	Description
Shunt regulator		
R_{sh}	Ω	Shunt current limiting resistor
I_K	A	Shunt cathode current
$I_{K_{\max}}$	A	Shunt maximum cathode current
$I_{K_{\min}}$	A	Shunt minimum cathode current
I_{su}	A	Shunt supply current
R_{A1}	Ω	Shunt adjust resistor 1
R_{A2}	Ω	Shunt adjust resistor 2
C_L	F	Shunt load capacitance
$V_{ref_{IC}}$	V	Shunt internal reference voltage

1 Introduction

The progress of diagnostic imaging has advanced significantly during the 20th century. As the cost of high speed computational systems has grown increasingly accessible, so has the use of medical imaging become prominent. Potentially millions of people have been spared painful exploratory surgery through non-invasive diagnostic imaging. And thus, lives can be saved by early diagnosis and intervention through medical imaging. Advancement in scientific visualization have in turn generated more complex datasets of increased size and quality. Four major technologies used are ultrasound (*US*), X-ray, computed tomography (*CT*), and magnetic resonance imaging (*MRI*). Each of the technologies have distinct advantages and disadvantages in biomedical imaging, thus each are still relevant for modern medicine. Table 1.1 contains a comparison and summary of the various fundamental diagnostic imaging modalities.

Table 1.1: Comparison of medical imaging modalities [18]

Modality	Ultrasound	X-ray	CT	MRI
Topic	Longitudinal, shear, mechanical properties	Mean X-ray tissue absorbtion	Local tissue X-ray absorbtion	Biochemistry (<i>T1</i> and <i>T2</i>)
Access	Small windows adequate	2 sides needed	Circumferential around body	Circumferential around body
Spatial resolution	0.2 mm 3 mm ^a	to ~ 1 mm	~ 1 mm	~ 1 mm
Penetration	3 cm to 25 cm ^b	Excellent	Excellent	Excellent
Safety	Excellent	Ionizing radiation	Ionizing radiation	Very good
Speed	Real-time	Minutes	20 minutes	Varies [†]
Cost	\$	\$	\$\$	\$\$\$
Portability	Excellent	Good	Poor	Poor
Volume coverage	Real-time volumes, improving	3D im-	2D	Large 3D volume
Contrast	Increasing (shear)	Limited	Limited	Slightly flexible
Intervention	Real-time increasing	3D	No ^c	Yes, limited
Functional	Functional ultrasound	ul-	No	fMRI

^a Frequency and axially dependent.

^b Frequency dependent.

^c Fluoroscopy limited.

[†] Typical: 45 minutes, fastest: Real-time (*low-res*).

Since medical imaging has been reportedly performed over 5 billion times as of 2004 [8],

and later numbers from 2011 show a general doubling, and particularly a ten-fold increase in ultrasound examinations between year 2000 and 2011 [18]. Recent data reveals that this trend of doubling has continued through the years 2010 to 2020 [26], and reveals that even though patient processes were disrupted during the global SARS-CoV-2 pandemic, the number of medical imaging examinations per 1000 patients, still increased. The reasons for this, and particularly why ultrasound has been notably increased in use, can be attributed to its high, but inconsistent, resolution, cost effectiveness, portability, and real-time interventional imaging. The downside of ultrasound is its limited penetration and restrictions for use in certain body parts. When just comparing soft-tissue examinations, which ultrasound is limited to, both *CT* and *MRI* can image the entire body with consistent resolution and contrast, but are more expensive and has poor portability due to immense size of its hardware.

The cardiovascular system, which transports oxygen and nutrients to tissue, produces a complex flow pattern that cause velocity fluctuations. Several cardiovascular diseases are also known to cause abnormal blood flow. As mentioned earlier, ultrasound is a powerful tool for conducting non-invasive imaging of the cardiovascular system [14], [17], and has no adverse risk to patients. Determining power spectral density (*PSD*) of a received signal is a common way to estimate blood velocity. A processed image of the *PSD* over time is commonly known as a sonogram, where changes in blood velocity over time can be seen.

1.1 Project scope

The aim of this project is to study the application of ultrasound in the context of blood flow measurements. Various scientific articles have been studied to gain knowledge of prior research [4]–[6], [9]–[13], [15], [16], [20]–[25]. In addition, the textbooks [17]–[19] have also been instrumental in forming a solid knowledge base for the thesis. The desire is to build upon the vast knowledge already gathered by prominent researchers in the field of ultrasound systems for blood velocity estimation. Finally, using the knowledge gained, to design and implement an electronic device capable of performing these measurements using a novel approach. The project specifications are written in table 1.2.

Table 1.2: Project specification table

Project specification
Study and research ultrasound and its principles and applications
Design and implement a device for ultrasound blood velocity estimation
Investigate and test the device in an experimental setting
Validate results with commercial equipment
Make quantifiable performance measurements on system
Write a technical report documenting the project work

The project is conducted under the guidance of advisors from the affiliated institutions Danmarks Tekniske Universitet (Technical University of Denmark) (*DTU*), Department of Electrical Engineering, Department of Applied Mathematics and Computer Science, and Korea Advanced Institute of Science and Technology (*KAIST*) at the Brain/Bio Medical Microsystems Laboratory.

The report is divided into five chapters, where the first part is an introduction to the project. The second chapter will focus on explaining the theory of the topic of the project.

The third chapter focuses on the synthesis of a system for experimental testing. The fourth chapter explains the production of the hardware. The fifth chapter will explain the testing methodology performed on the hardware. Finally, additional documentation of testing, code, circuit diagrams, and of laboratory setups can be found in the appendix.

2 Theory

2.1 Ultrasound

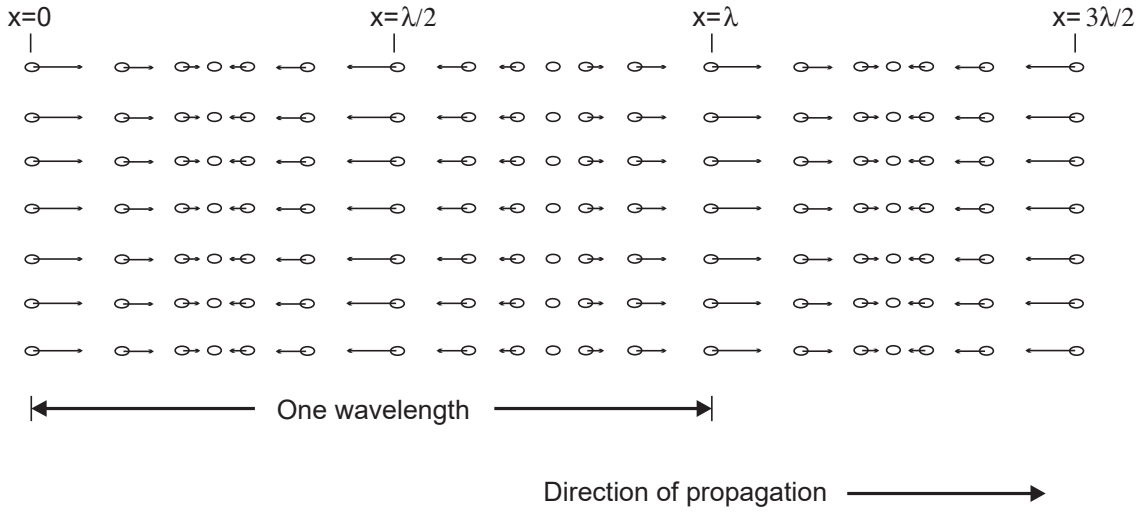


Figure 2.1: Particle displacement for a propagating ultrasound wave [17]

US is a technology that transmits sound waves with frequencies above the audible range (20 to 20 000 Hz) to mechanically vibrate matter. The particles in the medium would be at rest and distributed uniformly before any disturbance. The wave propagates as a disturbance and the particles oscillate around their mean position due to the presence of the ultrasonic wave. Typically the *US* frequency band used in clinical settings are from 1 to 15 MHz [18]. Figure 2.1 visualizes the propagation of a plane wave in matter. The oscillation occurs parallel to the wave's direction, making it longitudinal, and the disturbance will propagate with the variable c , which is determined by the medium and is given by eq. (2.1).

$$c = \sqrt{\frac{1}{\rho_0 \kappa_S}} \quad (2.1)$$

Where ρ_0 is the mean density (kg m^{-3}) and κ_S is the adiabatic compressibility ($\text{m}^2 \text{N}^{-1}$). Since in the majority of cases, the propagation of ultrasound is linear, it is assumed in this work. The acoustic pressure of the harmonic plane wave is expressed by eq. (2.2)

$$p(t, z) = p_0 e^{j(\omega t - kz)} \quad (2.2)$$

And propagates along the z -axis. ω is the angular frequency, k is the wave number and is expressed by $k = \omega/c = 2\pi/\lambda$, and p_0 is the acoustic pressure amplitude. A spherical wave is expressed by eq. (2.3)

$$p(t, r) = p_0 e^{j(\omega t - kr)} \quad (2.3)$$

Where r is radial distance, and is defined in a polar coordinate system. For each time instance, the acoustic pressure $p(t, r)$ is constant over a fixed radial position. In this scenario, the pressure amplitude is given by $p_0(r) = k_p/r$, where k_p is a constant since

the energy of the outgoing wave must be constant. Particle speed u is dependent on the pressure caused by a wave expressed by eq. (2.4)

$$u = \frac{p}{Z} \quad (2.4)$$

Where Z is the characteristic acoustic impedance, defined as the ratio of acoustic pressure to particle speed at a given position in the medium and is expressed by eq. (2.5).

$$Z = \rho_0 c \quad (2.5)$$

Characteristic acoustic impedance Z is one of the most significant variables in the characterization of propagating plane waves. Reference values for density, speed of sound, and characteristic acoustic impedance can be seen in table 2.1.

Table 2.1: Approximate density, sound speed, and acoustic impedance of human tissue types [17]

Medium	Density (ρ_0) kg/m ³	Speed of sound (c) m/s	Acoustic impedance (Z) kg/(m ² s)
Air	1.2	333	0.4×10^3
Blood	1.06×10^3	1566	1.66×10^6
Bone	$1.38\text{--}1.81 \times 10^3$	2070–5350	$3.75\text{--}7.38 \times 10^6$
Brain	1.03×10^3	1505–1612	$1.55\text{--}1.66 \times 10^6$
Fat	0.92×10^3	1446	1.33×10^6
Kidney	1.04×10^3	1567	1.62×10^6
Lung	0.4×10^3	650	0.26×10^6
Liver	1.06×10^3	1566	1.66×10^6
Muscle	1.07×10^3	1542–1626	$1.65\text{--}1.74 \times 10^6$
Spleen	1.06×10^3	1566	1.66×10^6

In the following sections, various acoustic wave phenomena will be briefly described.

2.1.1 Scattering

A wave propagating across a medium continues in the same direction until it encounters a new medium. When this occurs, a portion of the wave is transmitted into the new medium, with a change in direction. Because the scattered wave is the result of several contributors, it is necessary to define it statistically. The amplitude distribution is Gaussian [17] and can thus be fully described by its mean and variance. The mean value is zero because the dispersed signal is caused by variances of the acoustic characteristics in tissue. The correlation between multiple data is what allows ultrasound to determine blood velocities. Because minor movements have a significant correlation, it is feasible to discover alterations in location by comparing sequential measurements of moving structure, such as blood cells. In medical ultrasound, just one transducer is utilised for transmitting and receiving, and only the backscattered signal is analysed. The power of scattered signal is defined by the scattering cross-section, which in small cases mean a uniform intensity I_i , and is expressed by eq. (2.6).

$$P_s = I_i \sigma_{sc} \quad (2.6)$$

Where σ_{sc} is the scattering cross-section in square meters. The backscattering cross section is material dependant and determines the intensity of the scattering. If the dispersed energy is evenly emitted in all directions, the scattered intensity is given by eq. (2.7).

$$I_s = \frac{P_s}{4\pi R^2} = \frac{\sigma_{sc}}{4\pi R^2} \cdot I_i \quad (2.7)$$

Where R is distance to the scattering region [17]. This results in a spherical wave. A transducer with radius r gives the power P_r , presuming the attenuation and focus is neglected, and is expressed by eq. (2.8).

$$P_r = I_s \pi r^2 = \sigma_{sc} \frac{r^2}{4R^2} \cdot I_i \quad (2.8)$$

The backscattering coefficient, which characterizes scattering from a volume of scatterers, is another measure of scattering strength. It is defined as average received power per steradian volume of scatterers when flooded with plane waves of unit amplitude and the unit is 1/cm³sr. Back scattering coefficients in blood are significantly lower than the back scattering coefficients from various tissue types. This poses a challenge when estimating blood flow close to tissue vessel walls [3], [17].

2.1.2 Attenuation

The ultrasonic wave will be reduced as it propagates through tissue due to absorption and scattering. The attenuation in tissue is frequency dependent, with greater attenuation with increasing frequency. Because of absorption and dispersion, the ultrasonic wave will be attenuated as it travels through tissue. The relationship between attenuation, distance traveled, and frequency is frequently linear. Attenuation in tissue occurs as a result of both dispersion, which spreads energy in all directions, and absorption, which turns it to thermal energy.

Table 2.2: Approximate attenuation values for human tissue [17]

Tissue	Attenuation dB/(MHz · cm)
Liver	0.6–0.9
Kidney	0.8–1
Spleen	0.5–1
Fat	1–2
Blood	0.17–0.24
Plasma	0.01
Bone	16–23

The pressure of a wave propagating in z -direction decreases exponentially expressed by eq. (2.9)

$$p(z) = p(z = 0)e^{-\alpha z} \quad (2.9)$$

Where $p(z = 0)$ is the pressure in the point of origin and α is the attenuation coefficient. The attenuation coefficient unit is Npcm⁻¹ and alternatively, dBcm⁻¹ with the relationship described in eq. (2.10).

$$\alpha = \frac{1}{z} \ln \frac{p(z = 0)}{p(z)} \quad (2.10a)$$

$$\alpha(\text{dBcm}^{-1}) = 20(\log_{10}e)\alpha(\text{Npcm}^{-1}) = 8.68\alpha(\text{Npcm}^{-1}) \quad (2.10b)$$

The significance of absorption and scattering in ultrasonic attenuation in biological tissues is a point of contention. Scattering adds just a few percent to attenuation in most soft tissues. As a result, it is fair to conclude that absorption is the primary mechanism for ultrasonic attenuation in biological tissues [19].

2.1.3 Transducer

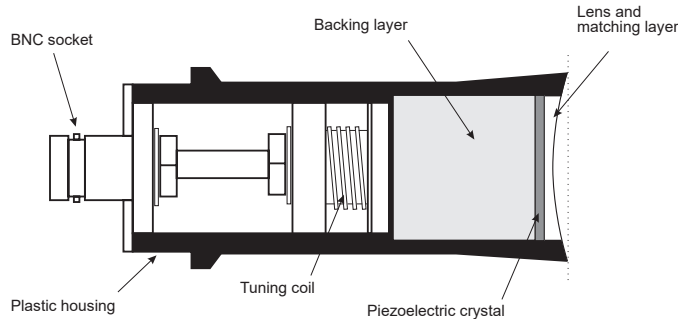


Figure 2.2: Single element ultrasound transducer construction [17]

A layperson knows transducers as speakers and microphones in the context of PA systems. In the case of medical *US* it is the device that generates the acoustic pressure field, which is emitted into tissue. The transducer has a piezoelectric crystal inside the housing. When excited, this crystal emits ultrasound waves toward flowing blood. The red blood cells will reflect a fraction of the emitted waves. These reflected waves are of a different frequency than the transmitted wave. If the red blood cells are moving away from the transducer, the frequency will be lower. If the red blood cells are moving towards the transducer, the frequency will be higher. This is caused by the Doppler effect. The reflected ultrasonic waves return to the crystal and are converted back into electrical signals. The single element transducer shown in fig. 2.2 has a minimal imaging window and has to be mechanically manipulated to get a wide window, which is unfeasible for responsive high-frequency imaging. Thus, usually an array transducer is used. Various *US* transducer types exist with different strengths and weaknesses, shown in fig. 2.3.

2.1.4 Doppler effect

The Doppler effect is a phenomena in which an observer perceives a shift in the frequency of sound emitted from a source when either the source or the observer is moving, or both are moving. The reason for the perceived change in frequency is visualised in fig. 2.4. In diagram (a), the source S_p is stationary and producing a spherical distribution pattern of the wave with the perceived frequency of the observer is given by $f = c/\lambda$, where c is the velocity of the wave in the medium and λ is the wavelength. In diagram (b), the sound source is moving towards the right with a velocity v . The locomotion of the source changes the distribution pattern and causes a longer wavelength on the left, indicating a lower perceived frequency, and a shorter wavelength on the right, indicating a higher perceived frequency, both denoted as λ' in the diagram. In the case of the observer on the right side, the perceived frequency becomes eq. (2.11).

$$f' = \frac{c}{\lambda} = \frac{c}{\lambda - vT} = \frac{c}{(c - v)T} = \frac{c}{c - v} \cdot f_0 \quad (2.11)$$

And viceversa, on the left side, the perceived frequency becomes eq. (2.12).

$$f' = \frac{c}{c + v} \cdot f_0 \quad (2.12)$$

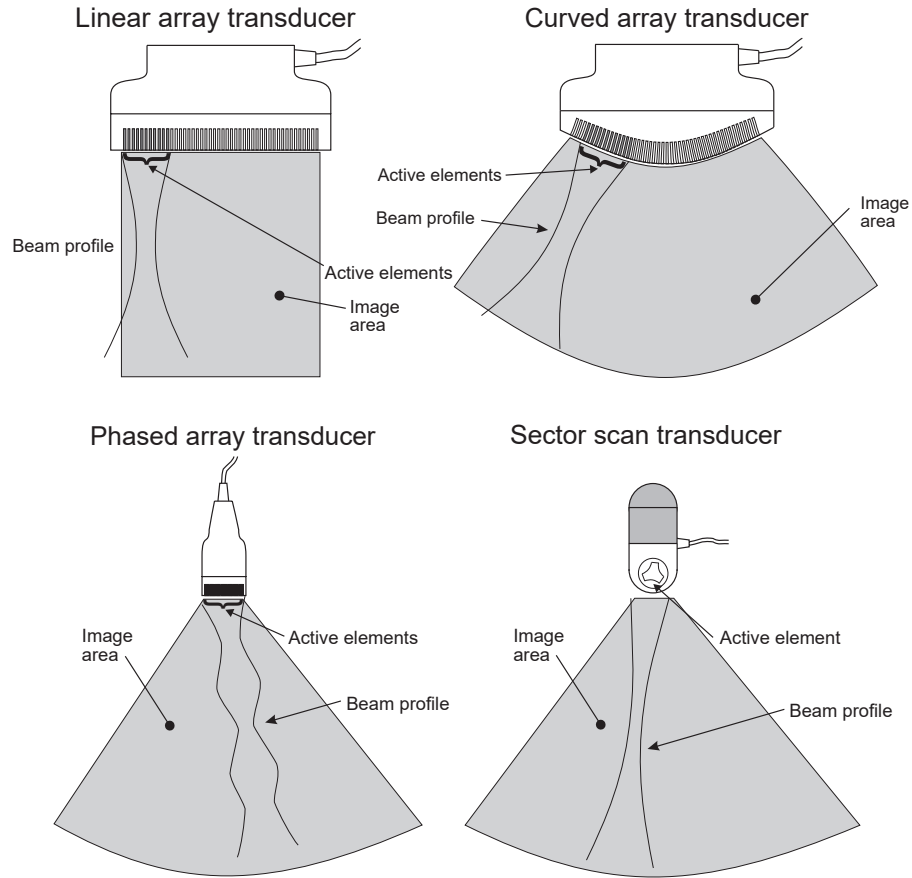


Figure 2.3: Transducer types for acquiring B-mode images [17]

Where

This perceived difference between the frequency that is transmitted from the source f_0 , and the perceived frequency f' is also called the Doppler frequency, f_d . When these connections are combined, the Doppler frequency for a source moving with velocity v and an observer traveling with velocity v' is given by eq. (2.13).

$$f_d = f' - f = \left(\frac{c + v'}{c - v} - 1 \right) \quad (2.13)$$

If both source and observer are moving with the same velocity, v , assuming $c \gg v$, the v cancels out and the expression is reduced to eq. (2.14).

$$f_d = \frac{2vf}{c} \quad (2.14)$$

If the velocity of the moving source is traveling with an incident angle θ , the v in eq. (2.14) is replaced with $v(\cos \theta)$. This results in the expression found in eq. (2.15) and forms the basis for applied Doppler effect measurements.

$$f_d = \frac{2v(\cos \theta)f}{c} \quad (2.15)$$

The Doppler effect is utilised in ultrasonic Doppler devices used to image blood flow transcutaneously. An ultrasonic transducer in these devices sends ultrasonic waves into a

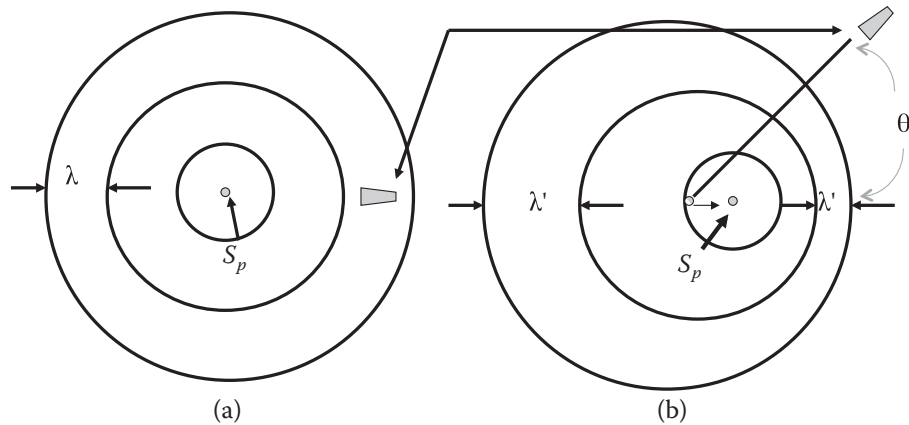


Figure 2.4: Doppler effect diagram. A stationary observer perceives a change in frequency of a wave generated by a moving source toward the observer as a result of a wavelength shift from λ to λ' . In (a), the source is still. In (b), the source is moving at a velocity v . [19]

blood artery, and the scattered radiation from moving red cells is measured by either the same transducer or a second transducer. The Doppler frequency, which is determined by the red blood cell velocity, is extracted using modern electronic demodulation techniques.

2.2 Flow physics

The flow physics of the human circulatory system are sophisticated and numerous non-stationary flow patterns emerge. The human circulatory system takes care of transporting oxygen and nutrients to the organs as well as disposing of waste products produced by metabolism. It is possible because the blood within the circulatory system contains several smaller subcomponents such as plasma and formed cellular elements that perform these vital functions. Initially, blood is discharged from the left ventricle of the heart via the aorta and travels to all areas of the body via multiple branches of the arterial tree. When the blood flows through the arteries, they into smaller channels known as arterioles. These arterioles lead into a network of tiny capillaries via which nutrients and waste materials are exchanged between the blood and the organs. The capillaries connect to form a network of venulae, which supply the veins, which deliver blood back to the heart. This system, in its totality, is called the systemic circulation. A diagram of the circulatory system as described above, can be seen in fig. 2.5. In summary, when examining the elements that comprise the circulatory system, it consists of several components:

- Heart, primary organ of the circulatory system that maintains blood pressure and controls blood velocity.
- Blood, and its sub-components
 - Plasma, which forms the primary volume and contains nutrients and formed cellular elements.
 - Red and white blood cells, which carry oxygen and fight off infections, respectively.
 - Platelets, which are also known as thrombocytes, with the function to clot during a blood vessel injury.

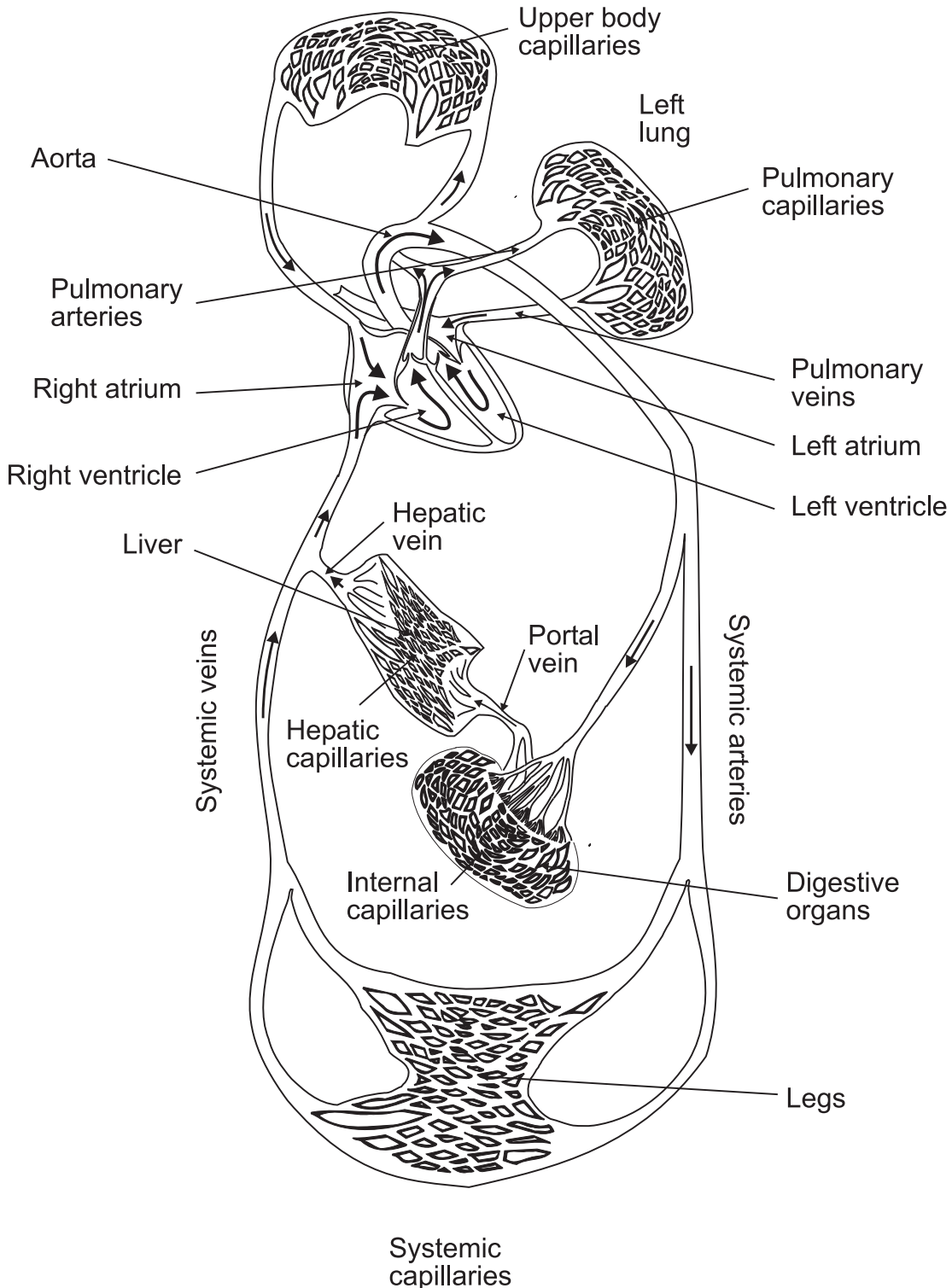


Figure 2.5: Circulatory system of the human body [17]

- Blood vessels
 - Arteries (and arterioles), that transport oxygenised blood to organs and tissues at high pressure and velocity.
 - Capillaries, thin but wide ranging blood vessels that performs the exchange of

matter between the circulatory system and tissue.

- Veins (and venules), carries blood back to the heart at low pressure and velocity.

2.2.1 Blood flow

Blood flow, which is the amount of blood that goes through a blood vessel in a particular period of time, and has a complicated flow pattern due to its pulsing flow. An advanced analysis of haemodynamics is not within the scope of this report, so the explanation will be brief. The primary forces that determines the blood flow F are the pressure difference across a blood vessel and vascular resistance. It is determined by Ohm's law as in eq. (2.16).

$$F = \frac{\Delta P}{R} \quad (2.16)$$

Where ΔP is the pressure difference across the blood vessel and R is the vascular resistance. The pressure difference ΔP is calculated with eq. (2.17).

$$\Delta P = P_1 - P_2 \quad (2.17)$$

Where P_1 and P_2 are the blood pressures measured at each end of the blood vessel. Pressure has a significant importance on blood flow because an increase in arterial pressure not only increases the force that pushes blood through the capillaries, but it also expands the vessels, lowering vascular resistance.

2.3 Devices

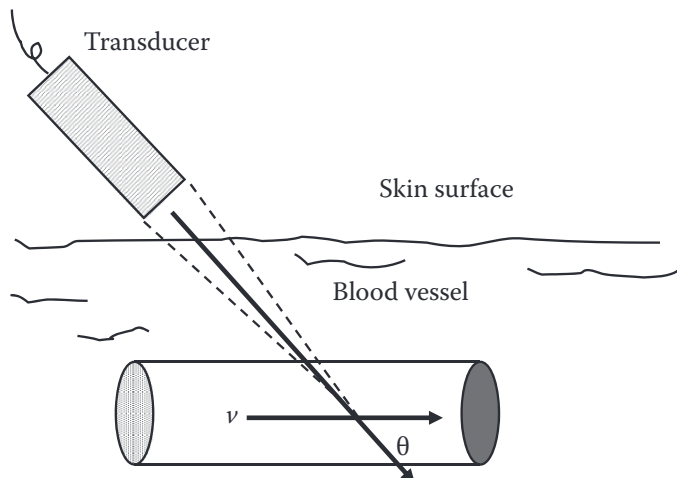


Figure 2.6: Diagram of *US* wave transmitted and reaching blood vessel with incident angle θ [19]

A device that measures the flowing of blood is called a flowmeter. Flowmeters may be used both inside and outside of vessels. One of the flowmeters that may be used outside the vessel to monitor flow is *US*. Figure 2.6 depicts an ultrasonic wave of frequency f insonifying a blood artery, resulting in an angle of θ relative to velocity v . For simplicity, it is assumed that blood flows in a vessel at a constant velocity v . The echoes returned are shifted in frequency as described in eq. (2.15) in earlier in the chapter. The echoes scattered by blood after being insonified by an ultrasonic wave convey information about the velocity of blood flow. Blood flow measurements are often used in clinical settings to determine the status of blood vessels and organ functioning. The two commonly used fundamental techniques for ultrasound Doppler flow measurements are continuous-wave (*CW*) and pulsed-wave (*PW*). Both will be explained.

2.3.1 Continuous-wave flowmeter

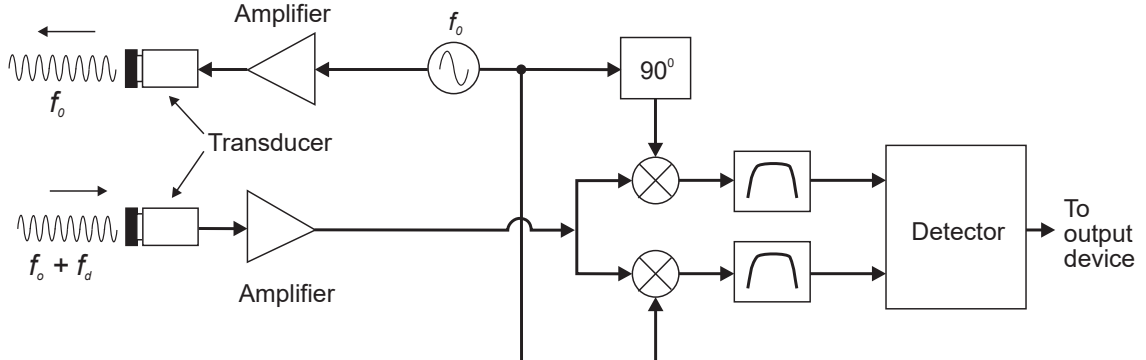


Figure 2.7: Block diagram of *CW* flowmeter [17]

The earliest non-invasive cardiovascular diagnostic technologies relied heavily on *CW* Doppler flowmeters. One of the earliest concepts for a device to estimate and study blood flow was proposed by Satomura, Yoshida, Mori, *et al.*[1] during the 1950's in Japan. To continuously transmit waves and receive signals from moving reflectors, the *CW* flowmeter uses two transducers. *CW* flowmeters use less sophisticated electronics than *PW* flowmeters. A drawback to the *CW* flowmeter is the lacking depth discrimination due to the continuous characteristic of this device type. A block diagram of a typical *CW* flowmeter can be seen in fig. 2.7. The basic principles of the device is previously explained in section 2.1.4, and the measurement of the device is described in eq. (2.11). The device continuously emits an ultrasonic wave in the first transducer expressed as a function of time by eq. (2.18) [17].

$$e(t) = \cos(2\pi f_0 t) \quad (2.18)$$

While receiving the backscattered signal on the second transducer expressed by eq. (2.19) [17].

$$r_s(t) = a \cos(2\pi f_0 \alpha(t - t_0)) \quad (2.19)$$

$$\alpha \approx 1 - \frac{2v_z}{c} \quad (2.20)$$

$$\alpha t_0 \approx \frac{2d_0}{c} \quad (2.21)$$

Where v_z indicates the velocity in the z -direction. Applying the Fourier transform, the expression yields eq. (2.22).

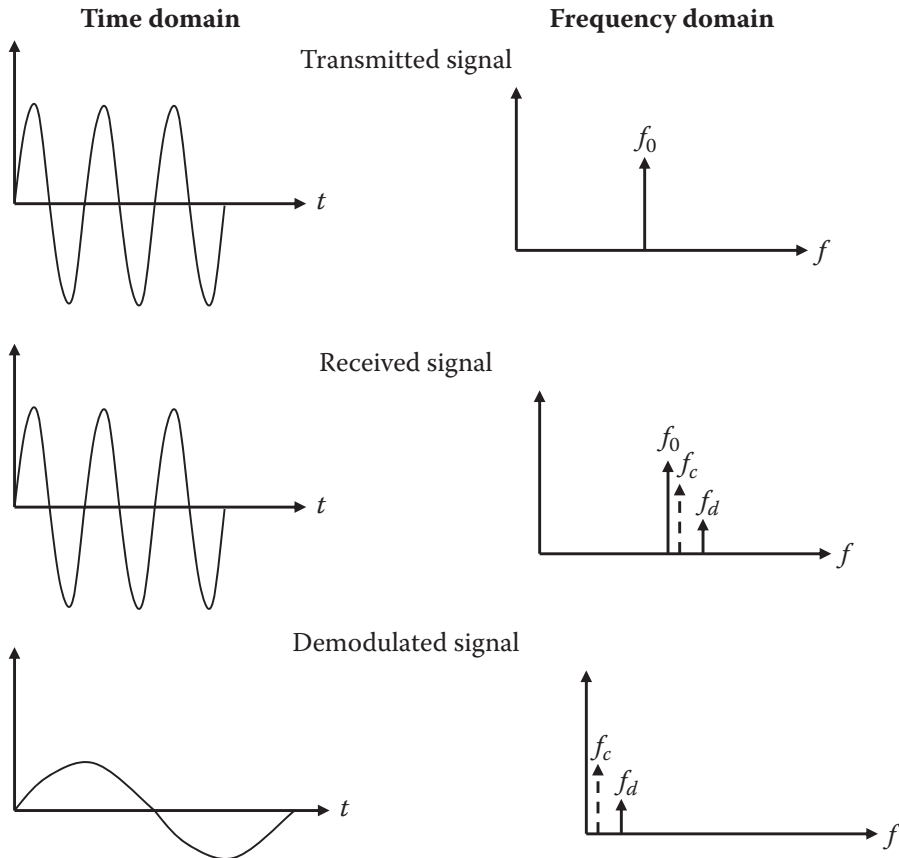
$$r_s(t) \cdot e^{j2\pi f_0 t} \iff R_s(f - f_0) \quad (2.22)$$

Where $R_s(f - f_0)$ is the Fourier transform of $r_s(t)$. The received signal is then multiplied with a quadrature signal of frequency f_0 to find the Doppler frequency in eq. (2.23).

$$m(t) = a [\cos(2\pi f_0 t) + j \sin(2\pi f_0 t)] \cos(2\pi f_0 \alpha(t - t_0)) \quad (2.23)$$

$$= \frac{a}{2} \left\{ \cos(2\pi f_0 [(1 - \alpha)t - \alpha t_0]) + \cos(2\pi f_0 [(1 - \alpha)t - \alpha t_0]) \right. \\ \left. + j \sin(2\pi f_0 [(1 - \alpha)t - \alpha t_0]) + j \sin(2\pi f_0 [(1 - \alpha)t - \alpha t_0]) \right\} \quad (2.24)$$

As is general for quadrature demodulation, the resulting signal contains the frequency components of the sum and difference of the emitted and received signals' frequencies shown in fig. 2.8, where the signals are shown in time and frequency domains.



f_c = Frequency of clutter signal e.g., from blood vessel wall

Figure 2.8: Doppler signals in time and frequency domain showing demodulation effects [19]

Generally a band-pass (*BP*) filter is used on the demodulated signal to remove the high frequency summed signal at twice the frequency of f_0 . The filtered signal after the *BP* filter is expressed by eq. (2.25) and contains the Doppler shift of the emitted signal.

$$m_f(t) \approx \frac{a}{2} e^{(j2\pi f_0 \frac{2v_z}{c} t)} e^{(-j2\pi f_0 \alpha t_0)} \quad (2.25)$$

Where the second exponential term is the delay proportional to the time between transmission and receiving of the signal. The selected cutoff frequency is chosen to be much lower than the carrier frequency to remove the carrier wave. One issue with ultrasonic Doppler blood flow monitoring is that the blood vessels that generate large reflected echoes are also moving with a low velocity. These big, slow-moving echoes are referred to as clutter signals in Doppler nomenclature. The band pass filter's low-end cutoff frequency must be designed to minimize interference from these clutter signals. The design of this band pass filter in the low-frequency region, which serves the function of high pass, also known as a clutter rejection filter, has proven troublesome since the magnitude of clutter signals is many orders greater than that of blood and may obfuscate those from slow-moving blood.

Seen in table 2.3 is an example of measured Doppler frequencies using a 3 MHz transducer using the method shown in fig. 2.6. Note that the frequencies measured are all within the audible range.

Table 2.3: Measured frequency shifts with a Doppler 3 MHz transducer at various velocities at a 45° incident angle [17]

Velocity (v) m/s	Doppler frequency (f_d) Hz
0.01	28
0.1	276
0.5	1377
1	2755
2	5510
5	13 770

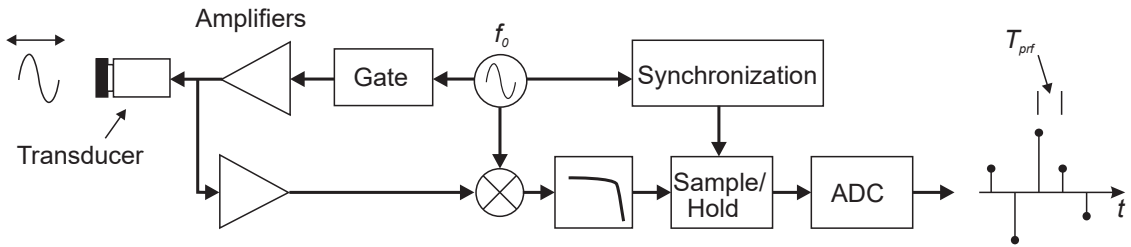


Figure 2.9: Block diagram of PW flowmeter [17]

2.3.2 Pulsed-wave flowmeter

The concept of a pulsed-wave flowmeter was proposed in [2] and other related articles. In this type of flowmeter is periodically changing from a transmitter to a receiver. In the transmitting mode, the transducer emits a series of pulses. When in the receiving mode, the transducer is listening for the back-scattered signal. A simplified block diagram can be seen in fig. 2.9. The movement of particles within the blood cause a displacement in the back-scattered signal. These systems are commonly referred to as “Doppler systems” even though it is somewhat misleading. The effects of attenuation is also causing a shift in frequency of a higher magnitude than the velocity of particles in blood. This is because the conventional Doppler effect is not the straight forward methodology that is applied to the analysis of the back-scattered signal. It is, in fact, an artifact. It is the shift in the location of the scatters that is observed, not the shift in the transmitted frequency. Figure 2.10 shows the received signal after demodulation and filtering; the depth in tissue is fixed here, and the signals displayed on the left side of the figure are the result of a pulse sequence. Each line represents a single pulse, and each pulse is emitted at a pulse repetition frequency, f_{prf} . Instead, on the right side, the dotted line shows the sampled signal formed by taking into account the amplitude of each pulse after a specified time period.

After the back-scattered signal is received it is multiplied by the center frequency of the emitted pulse and filtered to remove the sum frequency [17]. A analogue-to-digital converter (*ADC*) quantifies the signal for further signal processing. Referring to displacement fig. 2.10 again, the dashed vertical line represents the sample of each pulse that is taken. If sampling is done T_s after pulse emission, the measurement depth is expressed by eq. (2.26).

$$d_0 = \frac{T_s c}{2} \quad (2.26)$$

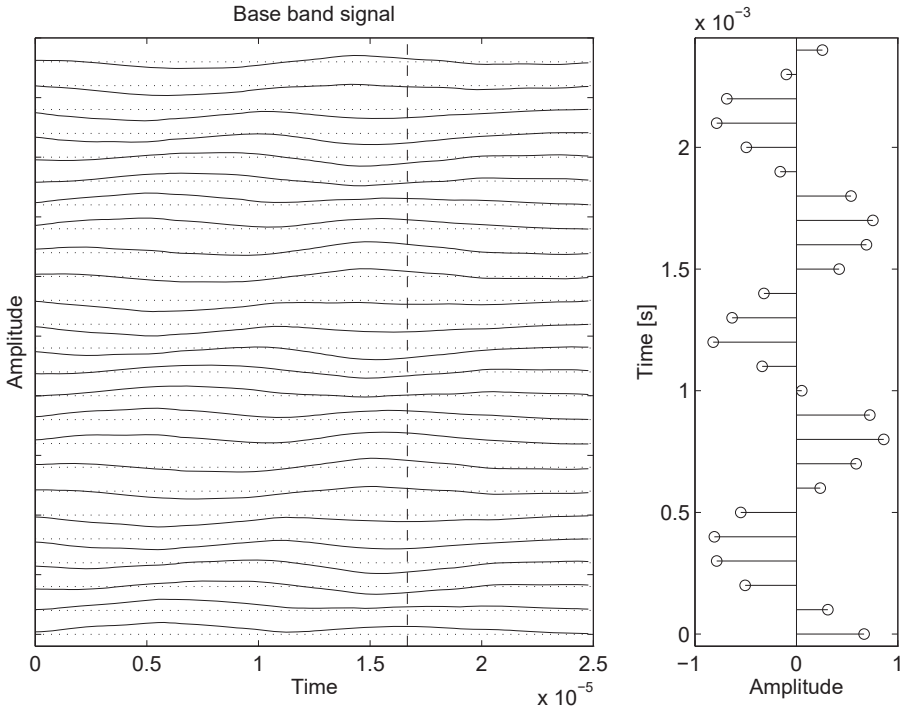


Figure 2.10: Sampling for a gate pulsed wave system with a single range. To depict the signals on the graph, a single pulse is emitted for each line, and the signals are displaced in amplitude. The sampled signal is displayed on the right. [17]

Hypothetically, if the velocity of stationary scatterers in blood was measured, a constant amplitude would be measured. A change in sample value is observed when movement is present. Between two pulses the scatterer movement is proportional to the velocity v_z in the direction of the ultrasound beam. Time shift of the t_s is expressed as eq. (2.27).

$$t_s = \frac{2v_z}{c} \cdot T_{\text{prf}} \quad (2.27)$$

Where c is the speed of sound, and T_{prf} is the timespan between each pulse emission. Taking one sample from each line at a certain depth yields a sampled signal with a frequency proportional to the scatter velocity. Thus, if a sample is taken at the same depth for each line, resulting in a sinusoidal signal proportional in frequency to the scatter velocity [7] and that signal is expressed by eqs. (2.28a) and (2.28b).

$$r(i) = a(i) \sin(2\pi f_p T_{\text{prf}} \cdot i) \quad (2.28a)$$

$$f_p = \frac{2v_z}{c} f_0 \quad (2.28b)$$

Where $a(i)$ is the amplitude, f_0 is the emitted frequency, and θ is the phase factor in the depth of interest. This technique improved the accuracy of the investigations of blood vessels and facilitated the display of velocity profiles. Furthermore, employing two transducers or a multi-element transducer, duplex mode imaging (displaying both a B-mode picture and a blood velocity estimate) became feasible. Two-transducer systems are no longer utilised, since it is easier to create a duplex picture with a multi-element transducer.

3 Synthesis

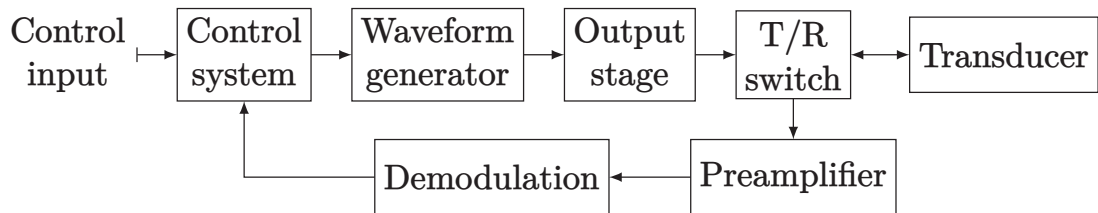


Figure 3.1: Simplified overview of the system

In the following a bunch of examples of figures and tables have been made. There are advantages to using `tikZ` diagrams over excel diagrams. 1) the font and font size perfectly matches the document 2) the styling and colours are pre-defined to follow the design guide 3) the plots uses vector graphics which reduces the file size, reduces the compile time and looks sharp when zooming in. The possibilities are endless, look at the `pgfplots` gallery for inspiration: <http://pgfplots.sourceforge.net/gallery.html>. However there are still cases where I would recommend to insert a plot as a picture. For example if the plot contains a lot of data: a line graph with 1000 points takes a long time to compile.

Remember to change the label of your figures so there are no duplicate labels. A label should be placed below a caption or after a heading (fx after a `\chapter`).

3.1 Graphs and charts

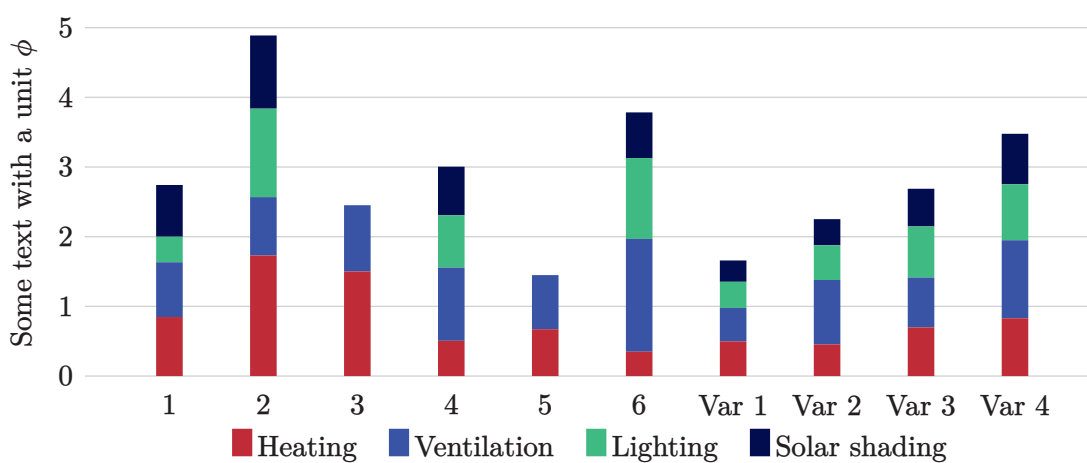


Figure 3.2: Stacked column chart

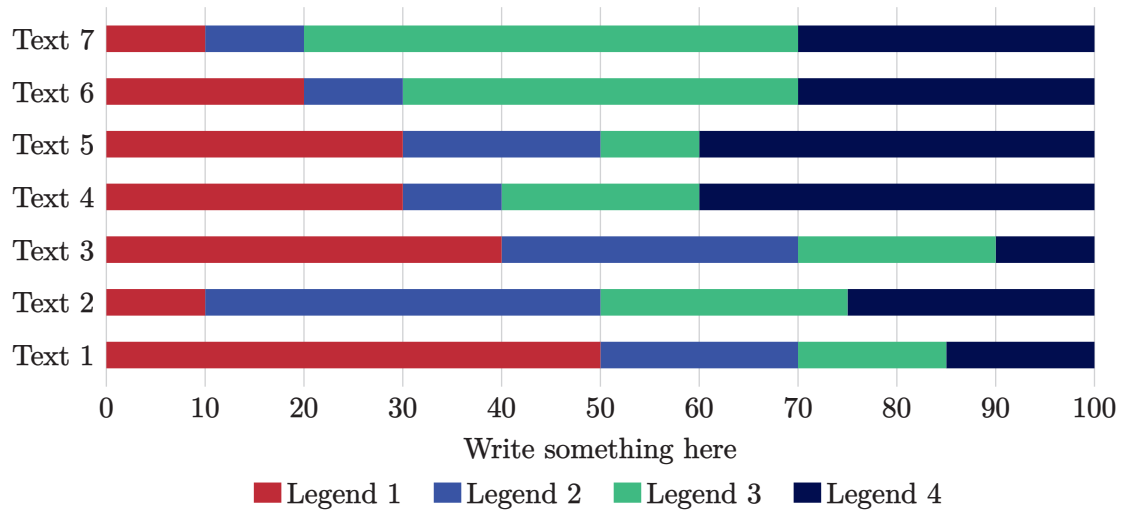


Figure 3.3: Stacked bar chart

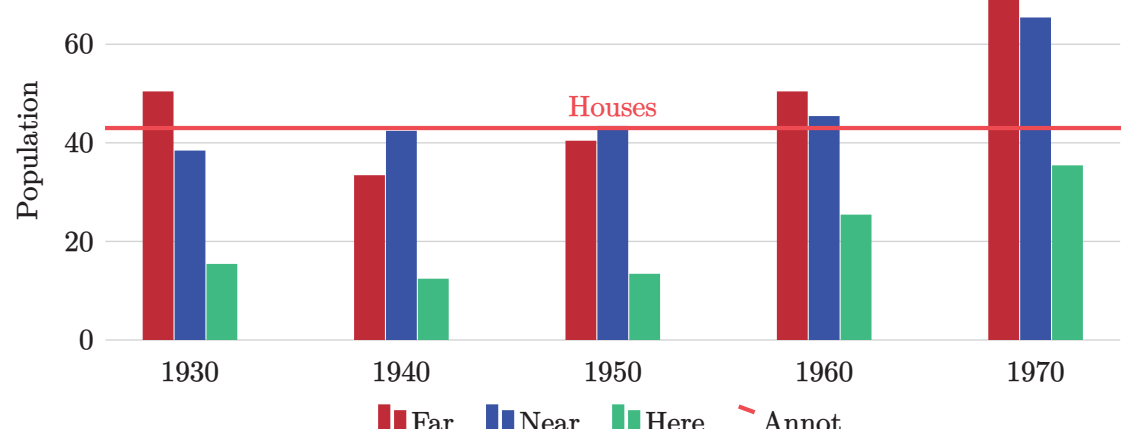


Figure 3.4: Grouped column chart

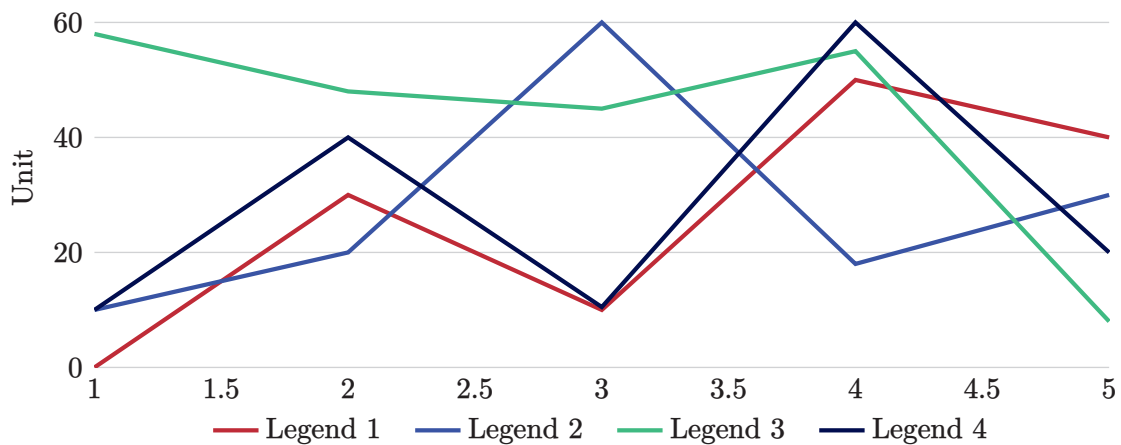


Figure 3.5: Line graph

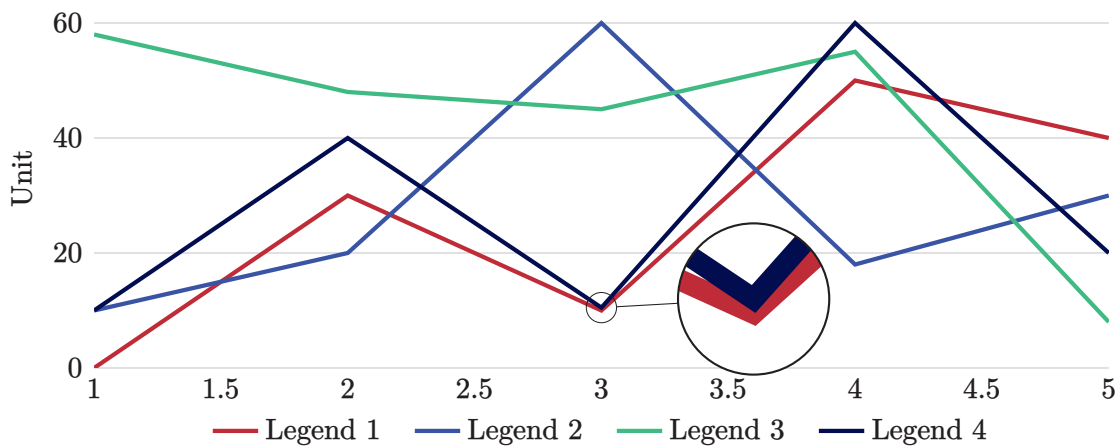


Figure 3.6: Line graph with magnifying glass

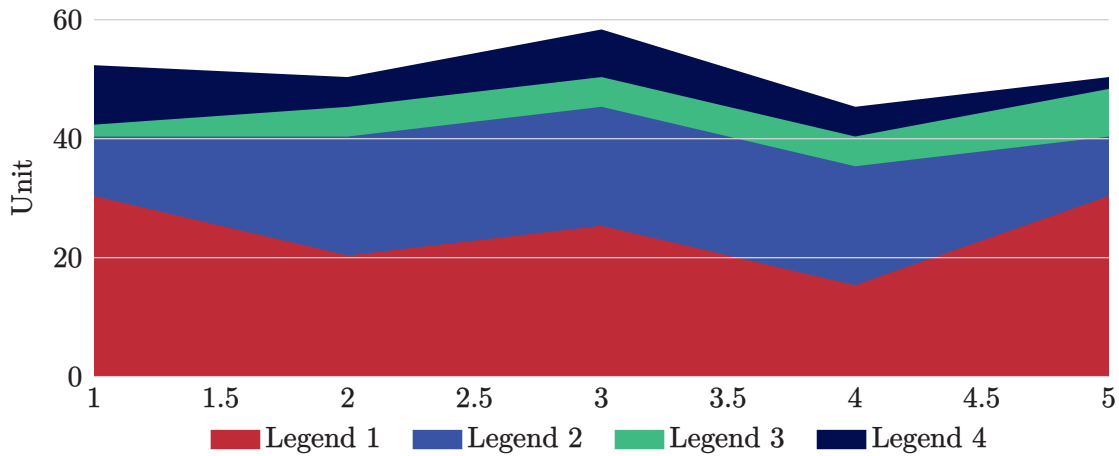


Figure 3.7: Area graph

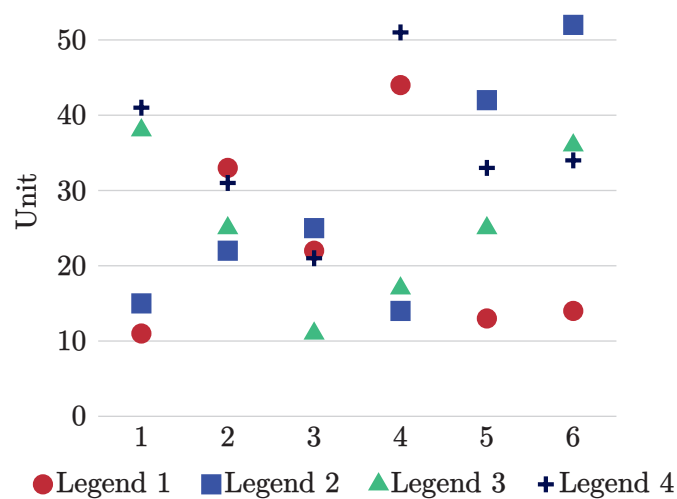


Figure 3.8: Scatter plot

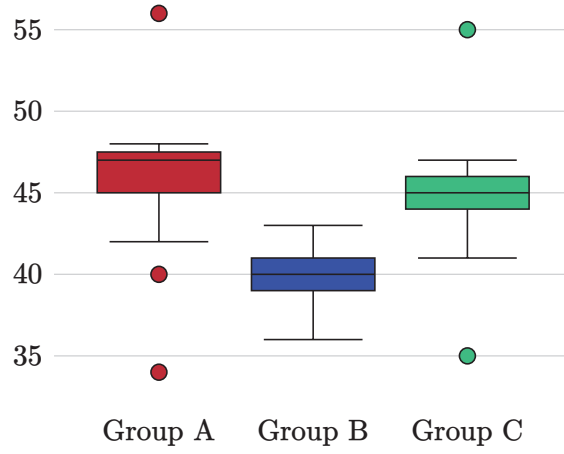


Figure 3.9: Boxplot

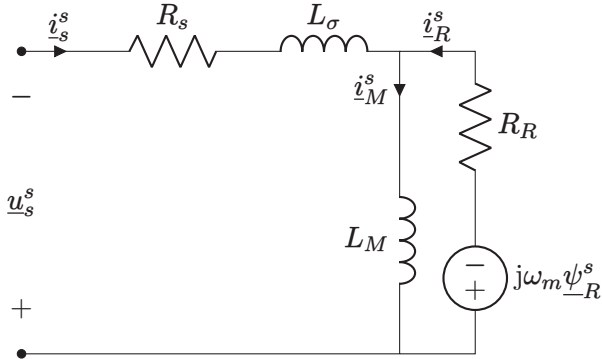


Figure 3.10: The nodes short, V, R and L are presented here, but there a lot more

3.2 Tables and figures

Table 3.1: This is a `booktabs` table

Animal	Description	Price (\$)
Gnat	per gram	13.65
	each	0.01
Gnu	stuffed	92.50
Emu	stuffed	33.33
Armadillo	frozen	8.99

Booktabs tables don't use any vertical lines. Only horizontal lines are used. Table 3.1 begins with a `\toprule`, ends with a `\bottomrule` with `\midrule` in between. The table has 3 columns formatted as `@{}l1S@{}`. `@{}` is cropping the horizontal lines of the table to fit the content (removes column spacing at the left and right edges). `l` aligns the column to the left and `S` aligns the column according to the decimal point (`siunitx` package). You can of course also use `r` to align right or `c` to center the contents of the column.

Table 3.2: Wrongly formatted table

	Voltage V	Current A	Power W
Transformer input	234.4	0.50	117.4
Transformer output	25.86	2.72	70.3
Efficiency	60%		

Table 3.3: Correctly formatted table

	Voltage V	Current A	Power W
Transformer input	234.4	0.50	117.4
Transformer output	25.86	2.72	70.3
Efficiency	60 %		

Table 3.2 and table 3.3 have the same contents but there are some subtle differences in formatting which makes table 3.3 the superior table of the two. The most obvious change is removing the midrule between the transformer input and output rows. The efficiency row is the odd man out and a midrule has been used to emphasise the difference between the transformer rows and the efficiency row. The delimiters in the voltage, current and power columns are aligned. The horizontal lines (rules) fits to the content and instead of protruding. The spacing between 60 and the percentage sign is correctly adjusted.



Figure 3.11: Just a normal figure



(a) A subfigure



(b) A subfigure

Figure 3.12: A figure with two subfigures



(a) A subfigure



(b) A subfigure



(c) A subfigure



(d) A subfigure

Figure 3.13: A figure with four subfigures

Referring to the figure as a whole fig. 3.13 or to an individual sub figure fig. 3.13a is done the normal way with `\cref{}` commands.

3.3 Equations

In-line math is easy. Anything surrounded by dollar signs becomes a math field. Here is an example: $f(x) = 2x - 1$. Also anything inside the “`\begin{equation}`” and “`\end{equation}`” environment is also a math field. Examples are shown below.

All equations use the default latex font. Some might say it looks weird with a serif font for equations and a sans-serif font for the body text. However, it is very unpractical to change the math font in latex which is the exactly the reason why this has not been done. One benefit of the serif style math font is the clear distinction between symbols (variables) and units.

On the subject of units, those are all taken care of by the `\siunitx` package. Whenever there is a number followed by a unit one should write `\SI{number}{unit}`. Note this

command is case sensitive. If a unit should follow a variable use the command `\si{unit}` (also case sensitive).

The ideal gas law is shown in eq. (3.1).

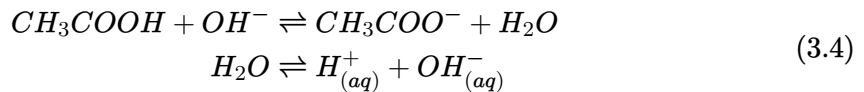
$$p \cdot V = n \cdot R \cdot T \quad (3.1)$$

$$\frac{\partial}{\partial t} \int_0^\delta U dy = -\delta \frac{1}{\rho} \frac{\partial P}{\partial x} - U_f(t)^2 \quad (3.2)$$

$$d_{step} = \sqrt{\frac{\delta}{\frac{dw}{dp_v}} \cdot t} = \sqrt{\frac{1 \text{ kg}/(\text{msPa})}{\frac{5.4 \text{ kg}/\text{m}^3}{233.82 \text{ Pa}}} \cdot 7200 \text{ s}} = 0.001766 \text{ m} = 1.766 \text{ mm} \quad (3.3)$$

$$x = x, x, x, x^{123^4} \cdot hello * \text{hello world} \cdot \text{equation without number}$$

Notice how the `aligned` environment can be used to align the equilibrium arrows in eq. (3.4). Only one equation number is generated using this method. Alternatively if you want an equation number for each line see eqs. (3.5) to (3.6).



$$f(x) = 1 + x - 3x^2 \quad (3.5)$$

$$g(x) + y = 3x - \frac{1}{2}x^3 \quad (3.6)$$

3.4 Listings (code)

Listing 3.1 is a nicely formatted block of code. A listing will automatically continue on the next page if it encounters a page break. Many different programming languages can be highlighted. Check the `listings` package documentation for a list of supported programming languages.

```

1  %% Monte Carlo simulation, estimation of pi
2  m=1E7;
3
4  x=rand(m,1);
5  y=rand(m,1);
6
7  g = x.^2+y.^2-1;
8
9  %dots outside
10 Pf = sum((g)<=0)/m
11
12 pi = 4*Pf

```

Listing 3.1: Monte Carlo simulation to estimate the value of π

Bibliography

- [1] S. Satomura, T. Yoshida, M. Mori, Y. Nimura, G.-i. Hikita, S. Takagishi, and K. Nakanishi, "Analysis of heart motion with ultrasonic Doppler method and its clinical application," *American Heart Journal*, vol. 61, pp. 61–75, 1 January 1961, ISSN: 00028703. DOI: 10.1016/0002-8703(61)90517-8. [Online]. Available: <https://linkinghub.elsevier.com/retrieve/pii/0002870361905178>.
- [2] D. Baker, "Pulsed Ultrasonic Doppler Blood-Flow Sensing," *IEEE Transactions on Sonics and Ultrasonics*, vol. 17, pp. 170–184, 3 Jul. 1970, ISSN: 0018-9537. DOI: 10.1109/t-su.1970.29558. [Online]. Available: <http://ieeexplore.ieee.org/document/1538563/>.
- [3] K. K. Shung and G. A. Thieme, *Ultrasonic scattering in biological tissues*. CRC Press, 1993, p. 499, ISBN: 9780849365683. [Online]. Available: <https://www.routledge.com/Ultrasonic-Scattering-in-Biological-Tissues/Shung-Thieme/p/book/9780849365683>.
- [4] J. A. Jensen, "An Analysis of Pulsed Wave Ultrasound Systems for Blood Velocity Estimation," *Acoustical Imaging*, L. T. Piero and Masotti, Eds., pp. 377–384, 1996. DOI: 10.1007/978-1-4419-8772-3_61. [Online]. Available: <http://link.springer.com/10.1007/978-1-4419-8772-3%5C%5F61>.
- [5] P. J. Fish, "Ultrasonic investigation of blood flow," *Proceedings of the Institution of Mechanical Engineers, Part H: Journal of Engineering in Medicine*, vol. 213, pp. 169–180, 3 March 1999, Pmid: 10420772. DOI: 10.1243/0954411991534898. [Online]. Available: <https://doi.org/10.1243/0954411991534898>.
- [6] T. Jansson, H. W. Peresson, and K. Lindström, "Estimation of blood perfusion using ultrasound," *Proceedings of the Institution of Mechanical Engineers, Part H: Journal of Engineering in Medicine*, vol. 213, pp. 193–193, 3 March 1999, ISSN: 0954-4119. DOI: 10.1243/0954411991534915. [Online]. Available: <http://journals.sagepub.com/doi/10.1243/0954411991534915>.
- [7] P. Munk, "Estimation of blood velocity vectors using ultrasound," Technical University of Denmark, 2000. [Online]. Available: <https://findit.dtu.dk/en/catalog/537f0d537401dbcc1200be04%20http://server.oersted.dtu.dk/publications/views/publication%5C%5Fdetails.php?id=827>.
- [8] E. Picano, "Sustainability of medical imaging," *Bmj*, vol. 328, pp. 578–580, 7439 March 2004, ISSN: 0959-8138. DOI: 10.1136/bmj.328.7439.578. [Online]. Available: <https://www.bmjjournals.org/lookup/doi/10.1136/bmj.328.7439.578>.
- [9] E. Chérin, R. Williams, A. Needles, G. Liu, C. White, A. S. Brown, Y.-Q. Zhou, and F. S. Foster, "Ultrahigh frame rate retrospective ultrasound microimaging and blood flow visualization in mice *in vivo*," *Ultrasound in Medicine & Biology*, vol. 32, pp. 683–691, 5 May 2006, ISSN: 03015629. DOI: 10.1016/j.ultrasmedbio.2005.12.015. [Online]. Available: <https://linkinghub.elsevier.com/retrieve/pii/S0301562906000172>.
- [10] X. Xu, J. Yen, and K. K. Shung, "A low-cost bipolar pulse generator for high-frequency ultrasound applications," *IEEE Transactions on Ultrasonics, Ferroelectrics and Frequency Control*, vol. 54, pp. 443–447, 2 February 2007, ISSN: 0885-3010. DOI: 10.1109/tuffc.2007.259. [Online]. Available: <http://ieeexplore.ieee.org/document/4107704/>.

- [11] I. K. H. Tsang, B. Y. S. Yiu, D. K. H. Cheung, H. C. T. Chiu, C. C. P. Cheung, and A. C. H. Yu, "Design of a multi-channel pre-beamform data acquisition system for an ultrasound research scanner," Ieee, Sep. 2009, pp. 1840–1843, ISBN: 978-1-4244-4389-5. DOI: 10.1109/ultsym.2009.5441869. [Online]. Available: <http://ieeexplore.ieee.org/document/5441869/>.
- [12] E. A. Aydn and . Güler, "Design Of Pic-controlled Pulsed Ultrasonic Transmitter For Measuring Gingiva Thickness," *Instrumentation Science & Technology*, vol. 38, pp. 411–420, 6 October 2010, ISSN: 1073-9149. DOI: 10.1080/10739149.2010.509149. [Online]. Available: <http://www.tandfonline.com/doi/abs/10.1080/10739149.2010.509149>.
- [13] N. Matsuoka, D.-G. Paeng, R. Chen, H. Ameri, W. Abdallah, Q. Zhou, A. Fawzi, K. K. Shung, and M. Humayun, "Ultrasonic Doppler measurements of blood flow velocity of rabbit retinal vessels using a 45-MHz needle transducer," *Graefe's Archive for Clinical and Experimental Ophthalmology*, vol. 248, pp. 675–680, 5 2010, ISSN: 1435-702x. DOI: 10.1007/s00417-009-1298-9. [Online]. Available: <https://doi.org/10.1007/s00417-009-1298-9>.
- [14] K. L. Hansen, M. B. Nielsen, and J. A. Jensen, "In-vivo studies of new vector velocity and adaptive spectral estimators in medical ultrasound," 2011. [Online]. Available: <https://orbit.dtu.dk/en/publications/in-vivo-studies-of-new-vector-velocity-and-adaptive-spectral-estimator>.
- [15] C.-C. Huang, P.-Y. Lee, P.-Y. Chen, and T.-Y. Liu, "Design and implementation of a smartphone-based portable ultrasound pulsed-wave doppler device for blood flow measurement," *IEEE Transactions on Ultrasonics, Ferroelectrics and Frequency Control*, vol. 59, pp. 182–188, 1 January 2012, ISSN: 0885-3010. DOI: 10.1109/tuffc.2012.2171. [Online]. Available: <http://ieeexplore.ieee.org/document/6138742/>.
- [16] C. A. Winckler, P. R. Smith, D. M. J. Cowell, O. Olagunju, and S. Freear, "The design of a high speed receiver system for an ultrasound array research platform," Ieee, October 2012, pp. 1481–1484, ISBN: 978-1-4673-4562-0. DOI: 10.1109/ultsym.2012.0370. [Online]. Available: <http://ieeexplore.ieee.org/document/6562380/>.
- [17] J. A. Jensen, *Estimation of Blood Velocities Using Ultrasound: A Signal Processing Approach*, Third Edition. Department of Electrical Engineering, Technical University of Denmark, August 2013, ISBN: 9780521464840.
- [18] T. L. Szabo, *Diagnostic Ultrasound Imaging: Inside Out*, Second Edition. Elsevier, 2014, ISBN: 9780123964878. DOI: 10.1016/c2011-0-07261-7. [Online]. Available: <https://linkinghub.elsevier.com/retrieve/pii/C20110072617>.
- [19] K. K. Shung, *Diagnostic Ultrasound: Imaging and Blood Flow Measurements*, Second Edition. CRC Press, December 2015, ISBN: 978-1-4665-8264-4.
- [20] P. Govindan, B. Wang, P. Ravi, and J. Saniie, "Hardware and software architectures for computationally efficient three-dimensional ultrasonic data compression," *IET Circuits, Devices & Systems*, vol. 10, pp. 54–61, 1 January 2016, ISSN: 1751-858x. DOI: 10.1049/iet-cds.2015.0083. [Online]. Available: <https://onlinelibrary.wiley.com/doi/10.1049/iet-cds.2015.0083>.
- [21] B. Wang and J. Saniie, "Ultrasonic Signal Acquisition and Processing platform based on Zynq SoC," vol. 2016-August, Ieee, May 2016, pp. 0448–0451, ISBN: 978-1-4673-9985-2. DOI: 10.1109/eit.2016.7535282. [Online]. Available: <http://ieeexplore.ieee.org/document/7535282/>.
- [22] B. Wang and J. Saniie, "A High Performance Ultrasonic System for Flaw Detection," Ieee, October 2019, pp. 840–843, ISBN: 978-1-7281-4596-9. DOI: 10.1109/ultsym.

- 2019 . 8926280. [Online]. Available: <https://ieeexplore.ieee.org/document/8926280/>.
- [23] H. Ding, D. Yang, J. Xu, X. Chen, X. Le, Y. Wang, L. Lin, and J. Xie, "Pulsed Wave Doppler Ultrasound Using 3.7 MHz Pmuts Toward Wearable Blood Flow Measurements," Ieee, January 2020, pp. 400–403, ISBN: 978-1-7281-3581-6. DOI: 10.1109/mems46641.2020.9056430. [Online]. Available: <https://ieeexplore.ieee.org/document/9056430/>.
- [24] B. Jana, R. Biswas, P. K. Nath, G. Saha, and S. Banerjee, "Smartphone-Based Point-of-Care System Using Continuous-Wave Portable Doppler," *IEEE Transactions on Instrumentation and Measurement*, vol. 69, pp. 8352–8361, 10 October 2020, ISSN: 0018-9456. DOI: 10.1109/tim.2020.2987654. [Online]. Available: <https://ieeexplore.ieee.org/document/9064842/>.
- [25] H. Ding, D. Yang, M. Qu, et al., "A Pulsed Wave Doppler Ultrasound Blood Flowmeter by PMUTs," *Journal of Microelectromechanical Systems*, vol. 30, pp. 680–682, 5 October 2021, ISSN: 1941-0158. DOI: 10.1109/jmems.2021.3103756. [Online]. Available: <https://ieeexplore.ieee.org/abstract/document/9515180>.
- [26] M. Winder, A. J. Owczarek, J. Chudek, J. Pilch-Kowalczyk, and J. Baron, "Are We Overdoing It? Changes in Diagnostic Imaging Workload during the Years 20102020 including the Impact of the SARS-CoV-2 Pandemic," *Healthcare*, vol. 9, p. 1557, 11 November 2021, ISSN: 2227-9032. DOI: 10.3390/healthcare9111557. [Online]. Available: <https://www.mdpi.com/2227-9032/9/11/1557>.

A Bill of Materials

Table A.1: Bill of Materials for the entire system

Component	Value	Footprint	Classification	Description
IO				
C1	1n	0603	X7R50V	Preamp
C13	1u	RAD-0.3in	Film 40V	Preamp
C14	1.5n	0603	X7R50V	PI controller
C15	NC	0603	X7R50V	PI controller
C2, C3, C4, C9, C10	100n	0603	X7R16V	Decoupling
C5, C11	1u	0603	X5R6.3V	Decoupling
C6, C7	100n	0805	X7R50V	Decoupling
C8	1500u	RAD-0.3in	63Vdc	Decoupling
P10	3-pin	Male	250V	Controller bypass
P11, P12	10-pin	Female	250V	InterPCB con.
P2, P3	1-pin header	Male	250V	Measurements
P4, P5	2-way screw	NA	300V 15A	30V Power, Output
P6	2-pin header	Molex KK254	500V 4A	Audio in
P7	4-pin header	Female	250V	5V Power
P8, P9	BNC	BNC PCB	500V	Audio in, Output
R2	16.2k	0603	1%	Preamp
R1, R3	2k	0603	1%	Preamp
R4, R7	4.75k	0603	1%	Voltage ref
R5	33.2k	0603	NA	PI controller
R6	0 (short)	0603	NA	PI controller
R9	0 (short)	0603	NA	PI controller
R10	NC	0603	NA	PI controller
R8	2.49k	0603	1%	Voltage ref
U1	OPA2365	SOIC-8	NA	Preamp, PI
U2	TLV431A	SOT-23	1%	Voltage ref

Table A.1: Bill of Materials for the entire system (Continued)

Component	Value	Footprint	Classification	Description
Power stage				
C1, C11, C15, C19	100n	0603	X7R16V	Gate driver
P1, P2	10-pin header	Male	250V	InterPCB con.
C2, C16	150n	0603	X5R10V	Gate driver
C3, C10	100p	0603	NPO50V	Decoupling
L1, L2	1.768u	Radial	NA	Output filter
U1, U3	LM5113	WSON-10	NA	Gate driver
R20	15m sense	1210	1% 1W	Output filter
R1, R6	500	SMDtrim 3213	NA	Gate driver
Q1, Q2, Q3, Q4	BSZ097-N10NS5	TSDSON-8	NA	Power stage
R2, R5, R8, R10	5	0603	1%	Gate driver
R4, R9	0	0603	1%	Gate driver
D1, D2	Diode	NA	85V 0.25A	Gate driver
C5, C6, C9, C17	10u	1210	X7R50V	Decoupling
C12, C13, C14	680n	1210	X7R100V	Output filter
AIM regulator				
C18,C20,C27	100n	0603	X7R16V	Decoupling
C28, C29, C30, C31	100n	0603	X7R16V	Decoupling
U6	LT1999	MSOP-8	NA	Current acq.
U4	AD8274	MSOP-8	NA	Volt acq.
U2	LT1711	MSOP-8	NA	AIM
C4	NC	0603	X7R16V	AIM
C7	NC	0603	X7R16V	AIM
C8	NC	0603	X7R16V	Cur. acq.
CA1	1.5n	0603	X7R50V	AIM
R14	8.66k	0603	1%	AIM
R18	16.2k	0603	1%	AIM
R23	1.5k	0603	1%	AIM
R3, R11	120k	0603	1%	Voltage acq.
RA1	2.2k	0603	1%	AIM
RA2	20k	0603	1%	AIM

Continued on next page

Table A.1: Bill of Materials for the entire system (Continued)

Component	Value	Footprint	Classification	Description
RA3	2.74k	0603	1%	AIM
RA4	0	0603	NA	AIM

B Instruments

Table B.1: List of instruments used for solder work

Function	Manufacturer	Model
Visual inspection microscope	Leica	A60
Manual soldering	Weller	WX2
Heat gun	Thermaltronics	TMT-HA600-2
SMT solder paste dispensing	Fisnar	SL101N
Reflow oven	Mistral	260
DMM	Meterman	38XR

Table B.2: List of instruments used for testing

Function	Manufacturer	Model
Power supply	RIGOL	DP832A
DMM	Agilent	34410A
Frequency response analysis	N4L	PSM1735
Audio analysis	Audio Precision	APx500
Audio analysis filter	Audio Precision	AUX-0025
Control loop analyzer	OMICRON Lab	BODE 100
Control loop injection transformer	OMICRON Lab	B-WIT 100
Passive load	Unknown	Power resistor 4Ω
Passive load	Unknown	Loudspeaker 4Ω
Active cooling	ebm	Test of bold

LOREM IPSUM

DOLOR SIT AMET, CONSECTETUER ADIPISCING ELIT.

Etiam lobortis facilisis sem. Nullam nec mi et neque pharetra sollicitudin. Praesent imperdiet mi nec ante. Donec ullamcorper, felis non sodales commodo, lectus velit ultrices augue, a dignissim nibh lectus placerat pede. Vivamus nunc nunc, molestie ut, ultricies vel, semper in, velit. Ut porttitor. Praesent in sapien. Lorem ipsum dolor sit amet, consectetur adipiscing elit. Duis fringilla tristique neque. Sed interdum libero ut metus. Pellentesque placerat. Nam rutrum augue a leo. Morbi sed elit sit amet ante lobortis sollicitudin. Praesent blandit blandit mauris. Praesent lectus tellus, aliquet aliquam, luctus a, egestas a, turpis. Mauris lacinia lorem sit amet ipsum. Nunc quis urna dictum turpis accumsan semper.

DTU Electrical Engineering
Technical University
of Denmark

%ørsteds Plads, Building 348
2800 Kgs. Lyngby
Tel. (+45) 4525 3800

www.elektro.dtu.dk

KAIST EE
Korea Advanced Institute
of Science & Technology

E3-2, 291
34141
Tel. (+82) 042-350-2114

www.ee.kaist.ac.kr